Available online at www.sciencedirect.com
SCIENCE DIRECT®
Journal of Chromatography A, 1074 (2005) 61–69
JOURNAL OF CHROMATOGRAPHY A
www.elsevier.com/locate/chroma

Estimation of diffusion parameters in functionalized silicas with modulated porosity Part II: Pore network modeling

G.S. Armatas, D.E. Petrakis, P.J. Pomonis *

Department of Chemistry, Dourouti, University of Ioannina, Ioannina 45 110, Greece

Received 16 September 2004; received in revised form 7 March 2005; accepted 10 March 2005
Available online 11 April 2005

Abstract

In this work, the pore structure of those five (5) silicas SiO_2–X (see Part I) which have suffered gradual functionalization with functional groups X of increasing length (X = Ø, ≡Si–H, ≡Si–CH_2OH, ≡Si–$(CH_2)_3$OH, ≡Si–$(CH_2)_{11}CH_3$), is modeled as a three-dimensional cubic network of cylindrical pores. Those hybrids organic–inorganic SiO_2–X samples are characterized by different extent of pore blocking effects. The pores of samples are represented in a $9 \times 9 \times 9$ lattice by the nodes as well the bonds that are interconnected in a so-called dual site-bond model, DSBM, network. The pore network is developed using a Monte Carlo statistical method where the cylindrical pores (nodes and bonds) are randomly assigned into the lattice, until matching of the theoretical results to the experimental data of N_2 adsorption–desorption measurements. Thus, a visual picture of the porous solid is possible. This realistic network is used next in order to study the steady-state gas transport (Knudsen gas-phase and viscous diffusion) properties for the examined materials and how flow processes depend on the morphology of the pore structure. The *pore diffusivity* D_p and *total permeability P* of each porous medium is determined based on theoretical calculations and the structural statistical parameters, such as porosity ε_p, tortuosity factor τ and connectivity c of pores is discussed with the corresponding experimental data described in Part I of this work. The results indicate clearly that the diffusion model made it possible to predict pore effective diffusivity in these porous media in very good agreement with the corresponding experimental results for all the examined solids (Part I). The pore diffusivity increases significantly as the value of the pore connectivity increases but the transport properties of the network are influenced strongly at lowest connectivity. Also the predicted tortuosity factor is related inversely to the extent of interconnection of pores in these solids, which indicates that the influence of pore branching to the tortuosity factor of the pore network decreases, as connectivity increases.

Keywords: Effective diffusivity; Porous solids; Porous network model

1. Introduction

The understanding of the relationship between the gas transport phenomena occurring within the void space of materials and into their pore structure is an important step in the design of new porous adsorbents and catalysts. Such problems are of great theoretical and practical interest for soil scientists, chemists and chemical and petrochemical engineers. The porous materials often possess complicated internal architecture with pores of various sizes and shapes interconnected in different arrangements. For this reason the problem of representing the porous structure and diffusion processes occurring within them is very complex. First, a detailed description of the materials must be sought using a suitable mathematical model. Second, a diffusion model that describes transport procedures must be applied at each pore of that porous model. While the local diffusion model provides successfully the dynamic and equilibrium properties for each pore, a convenient and/or simplified representation of the pore network is necessary for predicting the diffusion parameter and the transport properties in the whole porous system.

Frequently, the study of flow and transport processes in porous media is based on pore network model. One of the

* Corresponding author. Tel.: +32 651098350; fax: +32 651098795.
E-mail address: ppomonis@cc.uoi.gr (P.J. Pomonis).

0021-9673/$ – see front matter © 2005 Elsevier B.V. All rights reserved.
doi:10.1016/j.chroma.2005.03.091

most common network models developed, are those based on the so-called regular or random lattice. In this network model, a two- or three-dimensional lattice of nodes, which are interconnected by bonds, represent the pores of the real system. Models have been constructed from lattices categorized in two broad classes: (i) the pore bond models, consisting of a network of pore bonds [1–8] and (ii) the dual site-bond models, consisting of porous voids located at the nodes of the lattice with pore necks making the bond connections between these nodal sites [9–11]. Fitting such models to the experimental data may give information about the porous topology. Other models have suggested to represent the porous medium are the Bethe lattice [12–15] and the random packing of randomly placed spheres [16,17] or rods [18,19]. The flow and transport passes in such networks, take place through the channels between the overlapping or non-overlapping inclusions [20]. However, these particular types of models have highly convoluted and complex structures and are therefore difficult to be characterized fully using statistical parameters.

Discrete pore network models can be used in modeling transport processes such as single phase and two phase fluid flow, effective pore diffusivity and sorption phenomena [4,21–24]. In all cases, a mass balance equation for diffusion into the pores is set up and solved for the pore network. By calculating the concentration profile in the network, the transient diffusivity and the steady-state diffusivity are found. Bryntesson [25] has found that those two diffusivities are equal for three-dimensional networks when the connectivity has reached the percolation threshold of about 1.5. Also, it is true that if the connectivity of a regular network and the average connectivity of a random network are the same, the macroscopic properties of two networks are very close [26]. Therefore, it suffices to use cubic lattice and extending the bonds to connect second or higher nearest neighbors nodes.

In Part I, we studied the diffusion in five (5) functionalized silicas SiO_2–X. In Part II, the pore structure of those five (5) silicas SiO_2–X which have suffered gradual functionalization with functional groups X of increasing length (X = Ø, ≡Si–H, ≡Si–CH_2OH, ≡Si–$(CH_2)_3$OH, ≡Si–$(CH_2)_{11}CH_3$), is modeled as a three-dimensional cubic network of cylindrical pores. Those hybrids organic–inorganic SiO_2–X samples are characterized by different extent of pore blocking effects. The pores of samples are represented in lattice by the nodes as well the bonds that are interconnected. The pore network is developed using a Monte Carlo statistical method were cylindrical pores (nodes and bonds) are randomly assigned into the lattice, until theoretical results matching to experimental measurements [27]. Those networks are advantageous in several respects, especially for the distribution of connectivities in the pore space. Also local heterogeneities can be thus modeled and percolation phenomena in the network can be described. This realistic network is used here in order to study the steady-state gas transport (Knudsen gas-phase and viscous diffusion) properties for the examined materials and how flow processes depend on the morphology of the pore structure. The *pore diffusivity* D_p and *total permeability P* of each porous medium is determined based on theoretical calculations and the structural statistical parameters, such as porosity ε_p and connectivity c of pores is discussed. Also, the tortuosity factor τ is briefly discussed in the text. A further point of the present paper is a comparison between the predicted effective parameters, i.e. D_{eff}, based on the diffusion network model and the corresponding results found from the experimental measurements described in Part I of this work.

2. Model description

2.1. Pore network model

The pore structure of the solid was modeled as a regular three-dimensional cubic lattice of interconnected cylindrical pores. The maximum coordination number for a node in that cubic network is equal to 18 when one considers nearest neighbors only. The network surface is represented by two opposite faces of the network and periodic boundary conditions were applied at the other four faces. The pore walls were considered to be smooth. The pore volume of the solids was represent in the lattice from the nodes as well as from the bonds connecting the nodes. The pore radii, estimated from nitrogen adsorption measurements, are semi-randomly distributed over the nodes and the bonds of the co-called dual site-bond model, DSBM, network. Next, the relative arrangement of pores (nodes and bonds) changes according to a Monte Carlo methodology until the theoretical results simulate the experimental data of N_2 adsorption–desorption measurements. Thus, a visual picture of the porous solid is possible. Parameters that can be found from this model are the distributions of pore connectivities and the pore sizes as well as the average local tortuosity. For all the simulations presented in this work, a lattice size of $9 \times 9 \times 9$ was used, which provides a satisfactory representation of the pore network and does not require excessive computational time. Typical computation time for each sample was 1 week. Details of the network description and the method of computation there are in a previous publication [27].

The application of diffusion equations for each pore of the DSBM network was based on the following approach:

- The mean connectivity c_{mean}, the porosity ε_p, as well as the pore size distribution (PSD) are known parameters of the model.
- The flow through the network $(\vec{x}, \vec{y}, \vec{z})$ takes place along the z-direction perpendicular to $(\vec{x}, \vec{y})$ plane of the cube.
- The driving force of diffusion is the concentration gradient $\Delta C/l$ between the ends of pores. Through each pore, which is considered to have length l equal to their diameter d ($l = 2r = d$) [27], a linear change of the concentration is considered to take place. This is in agreement with experimental observations [22].
- The diffusion takes place in the pores of the network without adsorption phenomena.

To enable the calculation of effective properties, i.e. pore diffusivity and pore permeability, into the pore network model, we can use the bond network. In this case, the mass flux is proportional to the pore diffusion coefficient, to the bond cross-sectional area and finally to the difference between the concentrations of the connected nodes [25]. Thereafter, we changed the problem of double site-bonds network in simple bonds network, relating the volume of nodes to the volume of bonds according to the relation:

$$V_{\mathrm{n}} = \sum_{i=1}^{c} V'_{\mathrm{b}} \tag{1}$$

where V_{n} present the volume of node, c the connectivity of the node and Σ expresses the sum of additional volume V'_{b} that assign to the bonds connecting the node.

This approach is similar to bonds network model used by Meyers and Liapis [5,6] to calculate transport properties of small and large molecules in porous network.

2.2. Diffusion in single pores

The diffusion flow J of the dilute gas through a narrow cylindrical pore of radius r and length l, in the absence of adsorption, is given by the following equation [21]:

$$J = -\pi r^2 P \left(\frac{\Delta C}{l}\right) \tag{2}$$

where P is the permeability of the model pore ($\mathrm{cm^2\,s^{-1}}$) and ΔC is the difference of the gas concentration between the pore ends ($\mathrm{mol\,cm^{-3}}$). The minus sign in Eq. (2) means that as the diffusion is realized, the concentration gradient $\Delta C/l$ decreases.

Eq. (2) describes the diffusion that takes place in a pore with well-defined structure, as for example, in a straight cylindrical pore with smooth internal surface. Nevertheless, in a 3D pore network—as it is the case in real solids— in order to obtain the permeability P of the network in terms of diffusion, it is essential to express the total diffusion flow J_0 with the corresponding diffusion rates in each pore (Eq. (2)). This is achieved if we use a suitable mathematical model which represent satisfactorily the morphology of solid, as well as the pore volume distribution, the connectivity and finally the tortuosity of the pores.

The mass transport in the single pore is described as a sum of Knudsen J_{K} diffusion and viscous J_{V} flux:

$$J = J_{\mathrm{K}} + J_{\mathrm{V}} \tag{3}$$

The surface diffusion term can be included in Eq. (3) if necessary, although this mechanism of diffusion has not been taken into account in the model described here.

The Knudsen flux J_{K} is given by the following expression:

$$J_{\mathrm{K}} = -D_{\mathrm{K}} \frac{\mathrm{d}C}{\mathrm{d}z} \tag{4}$$

where D_{K} is the Knudsen diffusivity ($\mathrm{cm^2\,s^{-1}}$), which is correlated to the pore radius r according to Eq. (5).

$$D_{\mathrm{K}}(r) = \frac{2r}{3}\sqrt{\frac{8R_{\mathrm{g}}T}{\pi M}} \tag{5}$$

where r is the radius of pore (cm), R_{g} the universal gas constant ($8.314 \times 10^7\,\mathrm{g\,cm^2\,s^{-2}\,mol^{-1}\,K^{-1}}$), T the temperature of the system (K) and M is the molecular weight of fluid ($\mathrm{g\,mol^{-1}}$).

Under the influence of a pressure gradient along the pore, viscous flux occurs in addition to the diffusive flux. The viscous flux is given by:

$$J_{\mathrm{V}} = -D_{\mathrm{V}} \frac{\mathrm{d}C}{\mathrm{d}z} \tag{6}$$

where D_{V} is the viscous diffusivity ($\mathrm{cm^2\,s^{-1}}$), which is correlated to the pore radius r_{p} and the concentration C of fluid according to Poiseuille's law (Eq. (7)).

$$D_{\mathrm{V}}(r, C_{\mathrm{A}}) = R_{\mathrm{g}}T\frac{r^2}{8\eta}C \tag{7}$$

where η is the viscosity of fluid ($\mathrm{g\,cm^{-1}\,s^{-1}}$) and C is the vector of the concentration of the fluid into the nodes.

At the outer surfaces of the nodes of the network a boundary layer is assumed, perpendicular to the direction of flux. The top layer of nodes can be reduced to single node where the sum of the mass flux between this node and all of the remaining nodes into the network is equal to the specified total mass flux J'_0. Similarly, the bottom surface of the network can be reduced to a single node where the sum of the mass fluxes moving away from the nodes inside the network to this node is equal to the negative of the total specified mass flux, $-J'_0$ [5].

Then, for every interior node of network the fluxes of the gas that enter a node must be equal to the fluxes leaving the node. At the inner nodes of the network, an equation similar to Kirchhoff's law must be satisfied:

$$\sum_{j=1}^{n} J'_{ij} = \sum_{j=1}^{n} \frac{J_{ij}}{\pi r_{ij}^2} = \sum_{j=1}^{n} \left(P_{ij}\frac{C_i - C_j}{l_{ij}}\right)\delta_{ij} = 0 \tag{8}$$

where J'_{ij} represent the molar flow per unit cross sectional area of the bond b_{ij} perpendicular to the direction of flow between nodes i and j, P_{ij} the permeability of bond b_{ij}, C_i and C_j the concentrations of gas component at the nodes i and j, respectively, n the total number of nodes in the network, l_{ij} the length of pore bond b_{ij} and δ_j is a delta function that is equal to unity when the node i is connected by a pore to adjacent node j or equal to zero when is not connected.

The simultaneous solution of Eqs. (3)–(8) provides the concentration profile of gas fluid for each node of the network. The solution of these equations is reduced substantially in a problem of $n \times n$ non-linear equations:

$$\sum_{i} \mathbf{J}' = \mathbf{E}(r, C)\mathbf{C} = 0 \tag{9}$$

where $\mathbf{J}'$ present the vector of molar fluxes, $\mathbf{C}$ the vector of node concentrations and $\mathbf{E}$ is the square $n \times n$ matrix. Then the calculation of the Knudsen and the viscous diffusivities at each node of lattice, can be executed according to the following expression:

$$\mathbf{E}_{ij}(r_{ij}, C_i) = \begin{cases} \dfrac{2r_{ij}}{3l_{ij}}\sqrt{\dfrac{8R_gT}{\pi M}} + R_gT\dfrac{{r_{ij}}^2}{8l_{ij}\eta}\mathbf{C}_i, & \text{if } i \neq j \\ -\displaystyle\sum_{i\neq j}\frac{2r_i}{3l_i}\sqrt{\frac{8R_gT}{\pi M}} - \sum_{i\neq j} R_gT\frac{{r_i}^2}{8l_i\eta}\mathbf{C}_i, & \text{if } i \neq j \end{cases} \quad (10)$$

The diffusion model described above was coded in the ForTran 90/95 programming language in order to obtain the answers to the questions seeked. The non-linear equations for the single pores were solved using the ForTran MINPACK routine HYBRJ1, which applies the modified hybrid method of Powell [28]. The Jacobian was given in the algorithm for each node of the network.

In order to determine the pore diffusivity D_p of gas fluid in the porous network, we must first calculated the total permeability P of the lattice. The total permeability P includes the permeability of nodes as well as that of the bonds of the lattice according to the following relation:

$$P = \left(\frac{1}{2}\right)\left(\frac{1}{A_o}\right)\left[\sum_{i=1}^{n}\sum_{j=1}^{n}\left\{P_{ij}A_{ij} + \frac{P_iA_i}{c_i}\left(\frac{\Delta c_{ij}}{v_{ij}}\right)\right\}\right] \quad (11)$$

where the factor 1/2 is used because each pore is counted twice in the summation, A_{ij} and A_i the cross-sectional areas of bond $\pi(r_{ij})^2$ and node $\pi(r_i)^2$ perpendicular to the z-direction, respectively, c_i the number of bonds j that connected to the node i, A_o the cross-sectional area of the pores, v_{ij} represent the ratio of the pore length l_{ij} to the shortest distance connecting the node i with neighboring node j, and Δc_{ij} is the normalized concentration difference between nodes i and j, where

$$c_i = \frac{c_i - c_n}{c_1 - c_n} \text{ with boundary conditions } c_1 = 1 \text{ and } c_n = 0 \quad (12)$$

The cross-sectional area A_o for spherical particles diameter d_s is given by:

$$A_o = \frac{\pi d_s^2}{4}\left(\frac{1-\varepsilon_b}{\varepsilon_b}\right) \quad (13)$$

where d_s is the mean diameter of particles and ε_b is the porosity of the bed.

The permeabilities P_{ij} and P_i in Eq. (11) take into account the Knudsen diffusivity and the viscous diffusivity of bonds and nodes in the lattice, respectively, according to Eqs. (14a) and (14b).

$$P_{ij} = D_{K,ij}(r_{ij}) + D_{v,ij}(r_{ij}, C_i) \quad (14a)$$

$$P_i = D_{K,i}(r_i) + D_{v,i}(r_i, C_i) \quad (14b)$$

where $D_{K,ij}$, $D_{v,ij}$ and $D_{K,i}$, $D_{v,i}$ is the Knudsen and viscous diffusivities for the bond b_{ij} connecting nodes i and j and the node i, respectively.

The pores diffusivity D_p of the porous network for pure gas-phase transport is then obtained by:

$$\varepsilon_p D_p = P \quad (15)$$

where ε_p is the voidage of the lattice.

3. Results and discussion

3.1. Pore network model

The values of the mean connectivities c_{mean} obtained from the DSBM pore network estimated as described in ref. [27], as well as the values of the correlation coefficient R_{sq} corresponding to the best fitting between the simulated and experimental N_2-desorption curves, are show in Table 1. In the same table, the values of the voidage ε_p from the model and the porosity ε of the examined solids are cited. With this network model, we can determine the node/pore connectivity distribution of the network [27,29]. This kind of distributions—normalized to unity—is shown in Fig. 1 for all the samples. We observe that the connectivity values of pores/nodes, as well the c_{mean} ones, decrease in a systematic way with the extent of carbon length of the immobilized organic groups, as actually expected. This effect is due to the gradual blocking of the small pores by the organic groups. As a result the mean connectivity values drop significantly from $c_{mean} = 6.5$ at SiO_2 solids without functionalization to $c_{mean} = 3.6$ at SiO_2–$(CH_2)_{11}CH_3$ solids with functionalized group with maximum carbon length.

The estimation of the average tortuosity factor in the whole pore network model was also performed using the so-called local tortuosity method described elsewhere [27,29]. The values of those theoretically estimated tortuosity factors for all the examined solids are cited in Table 2. From these values it is rendered clear that the tortuosity increases with the pore blocking effects that affect the immobilized organic groups. In other words, the predicted tortuosity factor is related inversely to the extent of interconnection of pores for these solids. This means that the influence of pores branching on

Table 1
Pore network model parameters determined by matching the experimental nitrogen desorption data with the theoretical results obtained from DSBM simulations

Sample	c_{mean}	τ_p	ε_p	ε	R_{sq}[a]
SiO_2	6.5	4.7	0.67	0.66	0.9993
SiO_2–H	5.5	5.6	0.63	0.64	0.9989
SiO_2–CH_2OH	4.5	5.9	0.61	0.63	0.9990
SiO_2–$(CH_2)_3OH$	4.1	7.2	0.59	0.60	0.9991
SiO_2–$(CH_2)_{11}CH_3$	3.6	5.7	0.59	0.59	0.9991

[a] The simulations are realized in $9 \times 9 \times 9$ lattice size.

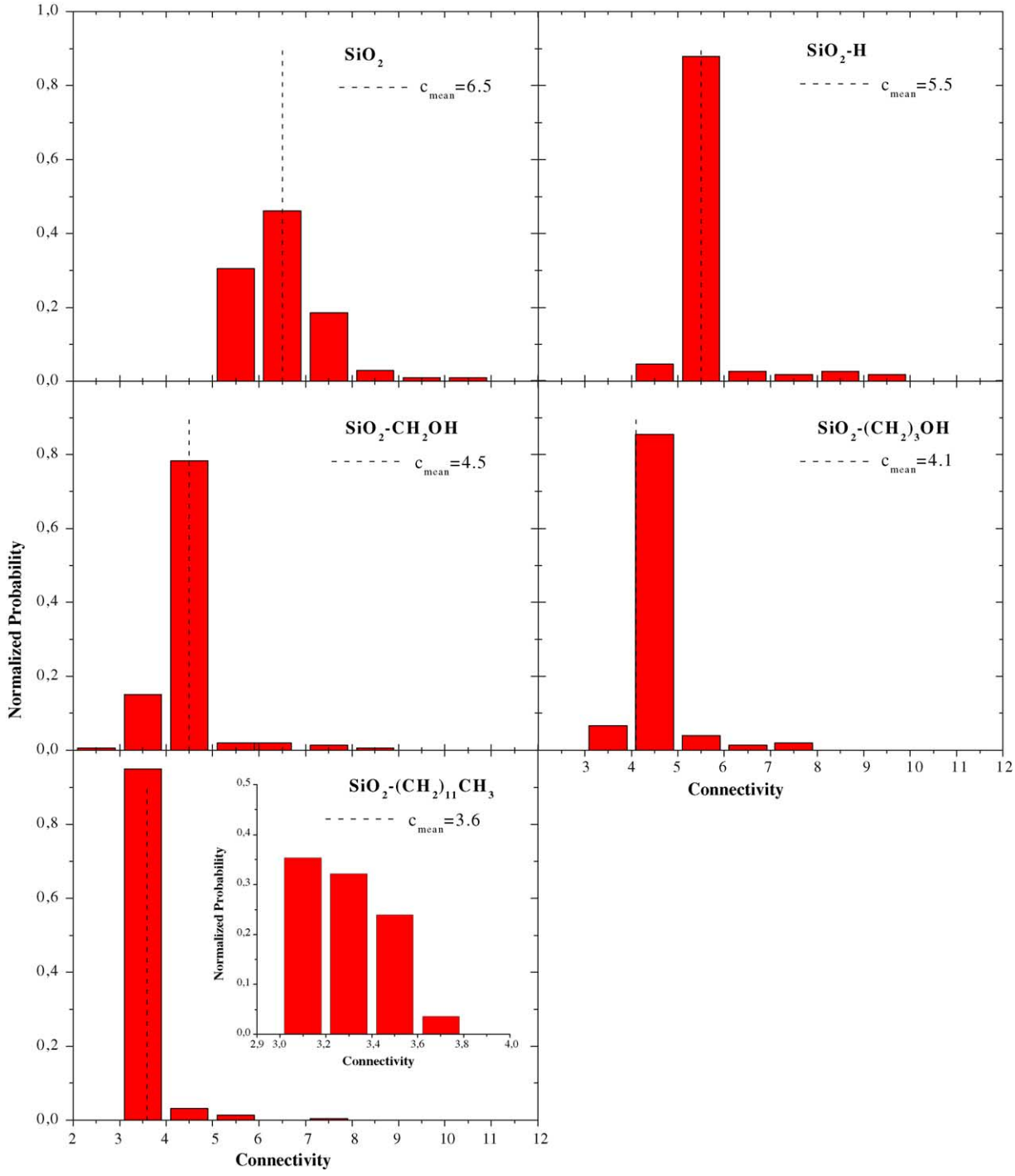

Fig. 1. The normalized to unity distribution of connectivities for the SiO_2–X sample. The c_{mean} values are also shown.

the tortuosity τ_p of pore network decreases, as connectivity increases. Those values of local tortuosities τ_p are affected in a similar way by functionalization as the corresponding tortuosities found from the experimental determination of τ with diffusion terms [30]. In Fig. 2, the variation of pore network tortuosity τ_p as well as the experimental tortuosity τ of the SiO_2–X solids are shown for comparison. The discrepancies between the τ_p and τ sets of values is attribute to the different approximations/simplifications which were taken into account for these methods, but the general the trend for the examined samples is similar in both cases.

In Fig. 3, two typical snapshots of the simulation of porous network are shown. The pores in that representation are not in scale because then it is not possible to distinguish the fine details of the network. The red line represents the percolation path of the network.

Table 2
Diffusion parameters of pure gas (He) flow in pore network DSBM for the SiO_2–X materials

Sample	Pore diffusivity, D_p[a] (10^{-3} cm^2 s^{-1})	Permeability, P[a] (10^{-3} cm^2 s^{-1})
SiO_2	2.486	1.575
SiO_2–H	2.003	1.282
SiO_2–CH_2OH	1.208	0.761
SiO_2–$(CH_2)_3OH$	1.102	0.650
SiO_2–$(CH_2)_{11}CH_3$	1.333	0.800

[a] The simulations were realized in $9 \times 9 \times 9$ lattice size with porosity of bed $\varepsilon_b = 0.3$, mean radius of particle $d_s = 1.0$ μm and viscosity of tracer gas (He) $\eta = 3 \times 10^{-4}$ g cm^{-1} s^{-1} [31].

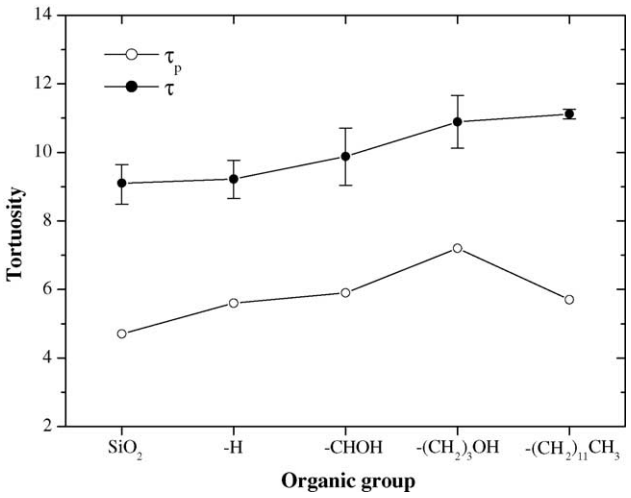

Fig. 2. Variation of the local tortuosities τ_p as well as of the experimental values τ [27] with the extend of pores blocking by the indicated organic groups.

3.2. Diffusion in the network model

Pore diffusion simulations of pure gas fluid (He) were performed using the modeling theory, as described above, in order to determine the pore diffusivity and the total permeability

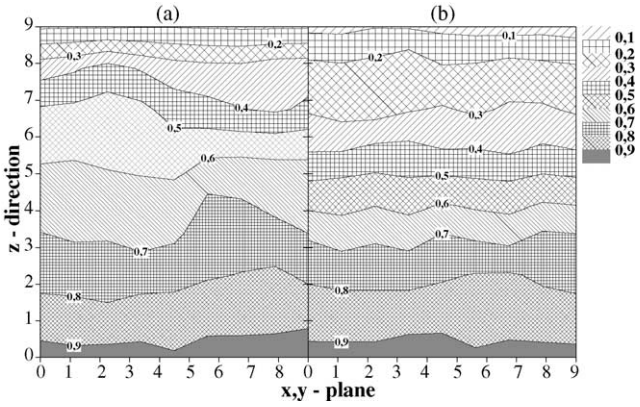

Fig. 4. Average concentration profiles in pore network model for (a) SiO_2 and (b) SiO_2–$(CH_2)_3OH$ samples. The fractions 0.1, 0.2, . . ., 1.0 correspond to the reduced concentrations of fluid (He).

of pore network model, DSBM. In Fig. 4, the calculated average concentration profiles normalized to unity, though the z-direction, for two typical sample SiO_2 and SiO_2–$(CH_2)_3OH$ are shown. We observed that the average concentration in (x, y) plane through the flow direction (z) drops more sharply for SiO_2–$(CH_2)_3OH$ than for SiO_2. This behavior is related to the restricted percolation effects because of the increased pore blocking that results from anchored organic residuals inside the pores of SiO_2 matrix.

The values of the estimated pore diffusivity D_p and total permeability P of the pore network model are mentioned in Table 2, for all the SiO_2–X solids. These results indicate clearly that the gas flow is substantially restricted from the immobilized organic groups SiO_2–X (X = –H, –(CH_2)OH, –$(CH_2)_3OH$ and –$(CH_2)_{11}CH_3$) inside the pores of hybrid solids. Namely, the pore diffusivity drops markedly from 2.5×10^{-3} cm^2 s^{-1} at SiO_2 to 1.1×10^{-3} cm^2 s^{-1} at SiO_2–$(CH_2)_3OH$ material. However, the pore diffusivity of SiO_2–$(CH_2)_{11}CH_3$ material with the greater immobilized carbon length is slightly increased relative to the previous sample. This discrepancy probably arises from the weakness of the model to forecast satisfactorily diffusion parameters in

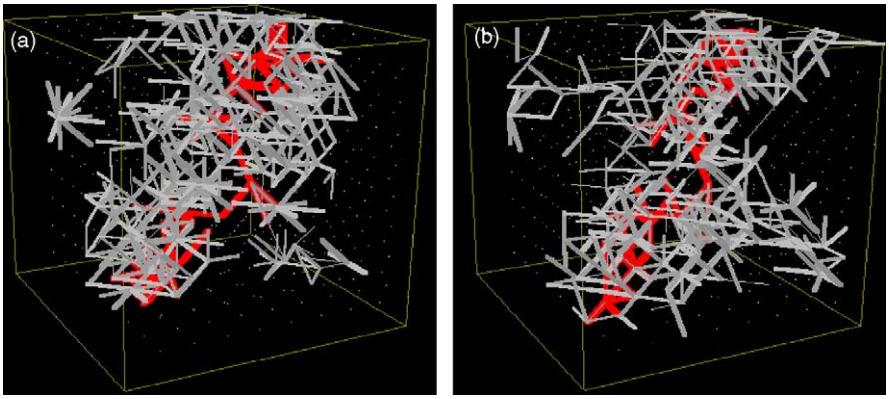

Fig. 3. Typical snapshots of the simulation of the network pores for the indicated sample: (a) SiO_2 and (b) SiO_2–$(CH_2)_3OH$. The red line corresponds to the percolation backbone of the network.

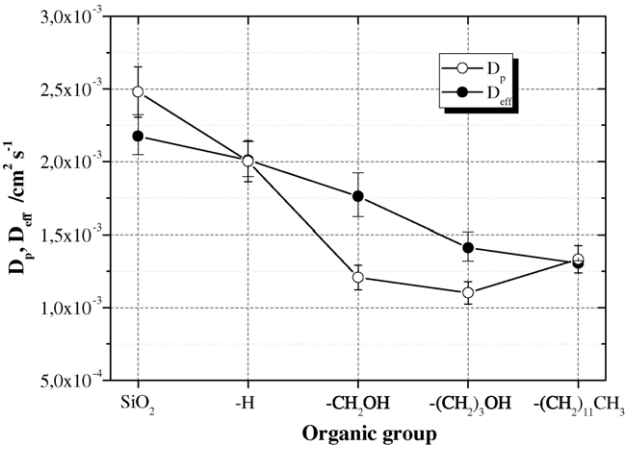

Fig. 5. Comparison plots between the predicted values D_p and the corresponding experimental values D_{eff} for the hybrid organic–inorganic SiO_2–X solids.

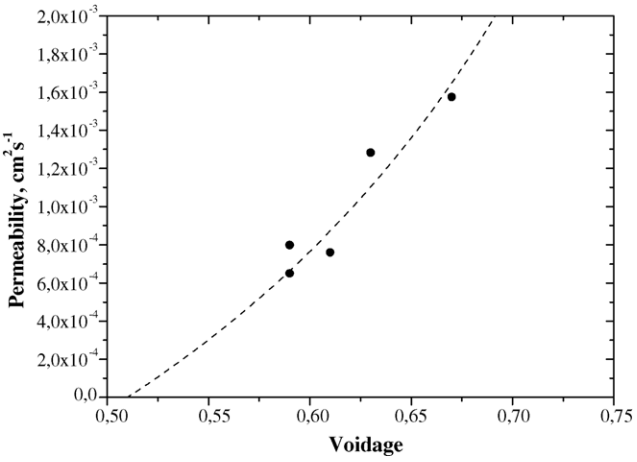

Fig. 6. Total permeability P of lattice as a function of the voidage of network. The dash line that simulates the data is given the empirical law, $y = A((x - v)/(1 - x))$ ($A = 3.3 \times 10^{-3}$ cm^2 s^{-1} and $v = 0.51$, $R_{sq} = 0.9128$), similar to the relation y $(x - 2/3)/(1 - x)$ found by Brosa and Stauffer [32] using random cellular automata model.

networks with low interconnectivity between the pores but in any case the precise reason is not very clear for the moment. In the case when the connectivity of pores is low, $c \sim 3$, the effectiveness of the network for diffusion is described in fractals terms. Similar cases have been reported by Bryntesson [25], who has calculated the pore effective diffusivity of solutes in poorly-connected networks. The simulations of the model porous network by Meyers and Liapis [5] also yield a percolation threshold at pore connectivity of 2.6. Below this value the system does not include a percolation cluster of interstitial pores which is necessary for flow through the porous model. The variation of the pore diffusivity for the examined solids is shown in Fig. 5. In the same figure, the variation of the corresponding pore diffusivity D_{eff} which was determinate from the experimental measurements in Part I [30], is shown for comparison.

We observe that the predicted reduction of pore diffusivity by the diffusion model is in very good agreement with the corresponding experimental results for all the solids.

The dependence of the total permeability P and pore diffusivity D_p from the voidage ε_p of the pore network for the SiO_2–X materials, are presented in Figs. 6 and 7, respectively. In Fig. 7, the variation of D_{eff} with porosity ε, found from the experimental measurements, is illustrated for comparison reasons.

It is clear that, both the theoretically pore diffusivity and the experimentally effective diffusivity varies essentially linearly with the voidage of pore network. Of course this suggestion constitutes a logical consequence of the diffusion processes, since the diffusion of fluid is realized more easily as the porosity of solids increases. Nevertheless, a very interesting point is related to the relative regression of parameters in Fig. 7. The formula of linear regression is a form $y = 16.8 \times 10^{-3}x - 8.7 \times 10^{-3}$. This relationship can be used to estimate pore diffusivity D_p for a particular voidage ε_p of the pore lattice. For example, at $\varepsilon_p = 1$ the pore diffusivity predicted equals $D_p \sim 8 \times 10^{-3}$ (cm^2 s^{-1}), the permeability of the system being very large at this point as seen in Fig. 6. We mentioned that the effective diffusion properties can be found only in the case where $\varepsilon_p > 0.5$ which corresponds to the percolation threshold. Before that point the permeability is zero (see Fig. 6). It should be noted that the relation between the pore diffusivity D_p and the voidage of lattice ε_p is influenced by the network topology and is valid for pore network system with similar mean connectivity. Indeed, the results for D_p—and much more for the D_{eff} values—can be represented by the empirical law, $D = (2p - 1)$, where D is the effective diffusivity normalized with respect to the value at porosity $p = 1$, as suggested by Sahimi and Stauffer for a triangular lattice [20]. Similar behavior between these parameters has been reported by other researches [33,34].

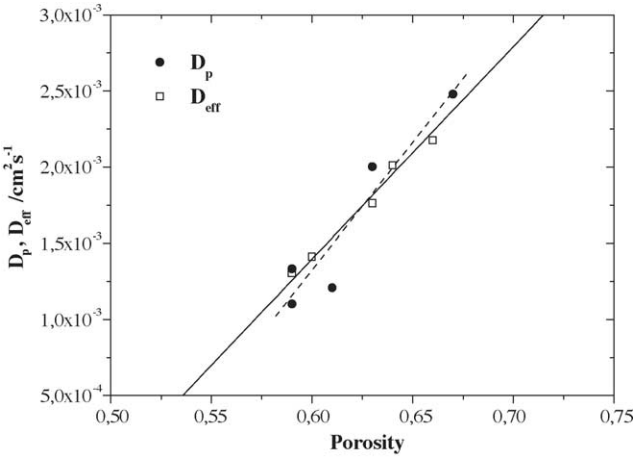

Fig. 7. Pore diffusivity D_p and effective diffusivity D_{eff} as a function of the voidage of lattice ε_p and the porosity ε of SiO_2–X solids, respectively. The dash line simulates the theoretical data by linear relation, $y = 16.8 \times 10^{-3}x - 8.7 \times 10^{-3}$ ($R_{sq} = 0.9467$) and the solid line give the empirical law, $y = A(2x - 1)$ ($A = 7.0 \times 10^{-3}$ cm^2 s^{-1}) similar to the relation found by Sahimi and Stauffer [20] in the triangular lattice.

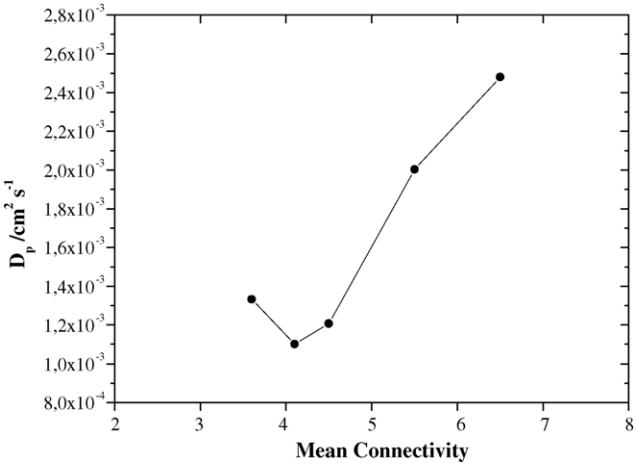

Fig. 8. Pore diffusivity D_p vs. the mean connectivity of the pore network model for examined solids.

In Fig. 8, the pore diffusivity D_p versus the mean pore connectivity c_{mean}, is illustrated, for the SiO_2–X solids. These results indicate clearly that for low values of the pores connectivity, the pore diffusivity is very low but at high values of connectivity the pore diffusivity is significantly enhanced. It can be observed that the increase of the pore diffusivity with c_{mean} in the range $4 < c_{mean} < 6.5$ is more significant. This result is due to the fact that the pores in the network are not interconnected significantly in the range 4–6.5, as to provide a good effective network. The connectivity must obtain higher values in order to allow for free transport through the pore network. Similar behavior between those parameters, i.e. pore diffusivity and pore connectivity have been reported by Meyers and Liapis [5], and Bryntesson [25]. Those authors have calculated transport properties in the pore network, near the percolation threshold, in the case when the size of solutes is comparable to the pore size.

This variation can be understood according to the suggestion that the diffusion resistance is strongest for the low connected pore network, but in the high-connected network the diffusion resistances are mainly due to pore size distribution and not to the networking topology.

4. Conclusions

In this paper we have described an efficient computation method for studying flow and transport process in porous media, using a dual site-bond lattice model, DSBM, of pore space. To be more precise we test the model using five (5) samples of mesoporous silica which suffered a gradual and controlled modulation of their porosity by functionalization with organic groups of various chain lengths. The diffusion model made it possible to predict pore effective diffusivity in these porous media in very good agreement with the corresponding experimental results for all the examined solids (Part I of this work). The simulations clearly indicate that the transport properties of the network are influenced strongly at lowest connectivity. Therefore, this last property is an extremely important parameter for the characterization and development of porous solids. The results show that the pore diffusivity increases significantly as the value of the pore connectivity increases. Also the tortuosity factor in the model porous network was estimated and compared to the tortuosity values calculated for the same materials with the experimental measurements (Part I of this work). It is rendered clear that tortuosity increases with the pore blocking effects from the immobilized organic residual inside the silicate pores. The predicted tortuosity factor is related inversely to the extent of interconnection of pores for these solids, which indicates that the influence of pores branching to the tortuosity factor of the pore network decreases, as connectivity increases.

Nomenclature

A	pore cross-sectional area (cm^2)
A_o	cross-sectional of pore network model (cm^2)
b_{ij}	pore-bond connecting nodes i and j
c	pore connectivity of the porous network
c	normalized to unity concentration ($mol\,cm^{-3}$)
C	node gas-phase concentrations ($mol\,cm^{-3}$)
C	vector of node concentrations ($mol\,cm^{-3}$)
d	pore diameter (cm)
D_K	Knudsen diffusivity ($cm^{-2}\,s^{-1}$)
D_p	pore diffusivity ($cm^2\,s^{-1}$)
D_v	viscous diffusivity ($cm^{-2}\,s^{-1}$)
J	molar flow ($mol\,cm^{-2}\,s^{-1}$)
J'	molar flux ($mol\,s^{-1}$)
$\mathbf{J}'$	vector of mole fluxes ($mol\,cm^{-2}\,s^{-1}$)
J'_0	total molar flux ($mol\,s^{-1}$)
J_0	total molar flow ($mol\,cm^{-2}\,s^{-1}$)
l	pore length (cm)
M	molecular weight ($g\,mol^{-1}$)
n	total number of pores in the lattice network
P	permeability of fluid in porous model ($cm^2\,s^{-1}$)
r	pore radius (cm)
R_g	universal gas constant ($g\,cm^2\,s^{-2}\,mol^{-1}\,K^{-1}$)
T	temperature (K)
V_b	bond-pore volume (cm^3)
V_n	node-pore volume (cm^3)
z	length coordinate (cm)

Greek letters

$\mathbf{E}$	matrix of diffusion coefficients factors
ΔC	concentration difference of gas between pore ends ($mol\,cm^{-3}$)
ε	porosity of solids
ε_b	porosity of bed
ε_p	voidage of lattice
η	viscosity of fluid ($g\,cm^{-1}\,s^{-1}$)
τ	mean local tortuosity factor
τ_p	tortuosity factor

Acknowledgements

We acknowledge financial support from EU under the project GROWTH—INORGPORE (G5RD-CT-2000-00317) and the PYTHAGORAS project of the Greek Ministry of Education.

References

[1] N.A. Seaton, Chem. Eng. Sci. 46 (1991) 1895.
[2] R.L. Portsmouth, L.F. Gladden, Chem. Eng. Sci. 46 (1991) 3023.
[3] A.O. Imdakm, M. Sahimi, Phys. Rev. 36 (A11) (1987) 5304.
[4] J.H. Petropoulos, A.I. Liapis, N.P. Kolliopoulos, N.K. Kanelopoulos, Bioseparation 1 (1990) 69.
[5] J.J. Meyers, A.I. Liapis, J. Chromatogr. A 827 (1998) 197.
[6] J.J. Meyers, A.I. Liapis, J. Chromatogr. A 852 (1999) 3.
[7] F.J. Keil, Chem. Eng. Sci. 51 (1996) 1543.
[8] R. Mann, A. Al-Lamy, A. Holt, I. Trans, Chem. E 73 (1995) 147.
[9] V. Mayagoitia, F. Rojas, I. Kornhauser, G. Zgrablich, R.J. Faccio, B. Gilot, C. Guiglion, Langmuir 12 (1996) 211.
[10] S. Cordero, F. Rojas, J.L. Riccardo, Colloids Surf. A: Phys. Eng. Asp. 187–188 (2001) 425.
[11] A.J. Ramirez-Cuesta, S. Cordero, F. Rojas, R.J. Faccio, J.L. Riccardo, J. Porous Mater. 8 (2001) 61.
[12] G. Mason, Proc. R. Soc. Lond. A 415 (1988) 453.
[13] J.W. Beeckman, G.F. Froment, Chem. Eng. Sci. 35 (1980) 805.
[14] S. Reyes, K. Jensen, Chem. Eng. Sci. 40 (1985) 1723.
[15] P.N. Sharratt, R. Mann, Chem. Eng. Sci. 42 (1987) 1565.
[16] S.C. Reyes, E. Iglesia, J. Catal. 129 (1991) 457.
[17] H. Drewry, N.A. Seaton, AIChEJ 41 (1995) 880.
[18] O. Mace, J. Wei, Ind. Eng. Chem. Res. 30 (1991) 909.
[19] B.J. Smith, J. Wei, J. Catal. 132 (1991) 41.
[20] M. Sahimi, D. Stauffer, Chem. Eng. Sci. 46 (1991) 2225.
[21] J.H. Petropoulos, J.K. Petrou, A.I. Liapis, Ind. Eng. Chem. Res. 29 (1991) 1281.
[22] F.A.L. Dullien, Porous, Media—Fluid Transport and Pore Structure, second ed., Academic Press, New York, 1992.
[23] M.P. Hollewand, L.F. Gladden, Chem. Eng. Sci. 47 (1992) 1761.
[24] K.-C. Loh, D.I.C. Wang, J. Chromotogr. A 718 (1995) 239.
[25] L.M. Bryntesson, J. Cromatogr. A 945 (2002) 103.
[26] G.R. Jerauld, L.E. Scriven, H.T. Davis, J. Phys. C 17 (1984) 3429.
[27] G.S. Armatas, P.J. Pomonis, Chem. Eng. Sci. 57 (2004) 5735.
[28] M.J.D. Powell, Numerical Methods for Nonlinear Algebraic Equations: A Hybrid Method for Nonlinear Equations, Gordon and Breach, 1970.
[29] G.S. Armatas, Synthesis, Surface Functionalization of Porous Solids and Study of their Pore Structure, Ph.D. thesis, University of Ioannina, Ioannina, 2003.
[30] Part I of present paper.
[31] R.C. Weast, HandBook of Chemistry and Physics, 55th ed., CRC Press, Cleveland, Ohio, 1974.
[32] U. Brosa, D. Stauffer, J. Stat. Phys. 62 (1991) 399.
[33] C.N. Satterfield, Mass Transfer in Heterogeneous Catalysis, M.I.T. Press, Cambridge, MA, 1970.
[34] R. Vocka, M.A. Dubois, Phys. Rew. E 62 (2000) 5216.